Marangoni Convection in a Fluid Layer over Anisotropic Porous Media: An Exact Solution Approach

Padmavathi Ramanna[1] , Rashmi K[2] , Ambika H V[3] , Srihari M Subodha[4,*] , Dhruvathara B S[4]

[1] Department of Mathematics, Nitte Meenakshi Institute of Technology, Nitte University Campus, Post Box no. 6429, Govindapura, Yelahanka, Bengaluru 560064, India

[2] Department of Agricultural Statistics, Applied Mathematics & Computer Science, University of Agricultural Science, GKVK, Bengaluru 560065, India

[3] Department of Mathematics, Cambridge Institute of Technology, Krishnarajapuram, Bengaluru 560036, India

[4] Department of Mathematics, RNS Institute of Technology, Dr. Vishnuvardhan Road, Channasandra, Rajarajeshwari Nagar, Bengaluru 560098, India

[*] Corresponding Author: Srihari M Subodha
Email: sriharimsubodha@gmail.com

Marangoni Convection in a Fluid Layer over Anisotropic Porous Media: An Exact Solution Approach

Abstract

Exact analytical solutions are derived for velocity fields and Marangoni number in a fluid layer overlying an anisotropic porous medium, incorporating the effects of internal heat generation and couple stresses. Parametric evaluation of the closed-form results shows that enhancement-type parameters (a,b,ξ) amplify velocities and Marangoni numbers, the resistance-like parameter λ suppresses them, and Q has only a weak influence; the Marangoni number exhibits an approximately exponential decay with fluid-layer thickness. In addition, a reduction in couple-stress is found to increase fluid velocity, while internal heat generation strengthens thermocapillary-driven motion in the fluid layer though its impact within the porous layer depends on the relative layer depths. The exact solutions provide clear physical insight and quantitative benchmarks useful for the design of thermal-management, coating, and microgravity applications where surface-tension-driven transport is important.

Keywords: Marangoni convection, Anisotropic porous medium, Exact solutions, Thermocapillary flow, Fluid–porous layers.

1. Introduction

Thermocapillary-driven convection, commonly known as Marangoni convection, arises from gradients of surface tension at fluid–gas interfaces and plays a crucial role in microscale heat and mass transfer. The classical foundation of this phenomenon was laid by Scriven and Sternling [9], who demonstrated the destabilizing influence of surface-tension gradients on fluid layers, and by Koschmieder and Biggerstaff [10], who analysed the onset of surface-tension-driven Bénard convection. Since then, a rich body of literature has examined Marangoni convection under varied physical effects, including porous substrates, magnetic fields, ferrofluids, nanofluids, and hybrid thermal–fluid systems.

The interaction between a pure fluid layer and an underlying porous medium has drawn particular attention due to its relevance in coating, crystal growth, and microgravity applications. Kozak et al. [1] investigated Marangoni convection in a liquid layer overlying a porous layer with surface evaporation, while Saghir et al. [2] reported transient convection patterns in coupled fluid–porous configurations. Building upon these foundations, Abdullah and Rashed [3] analysed the instability of Bénard–Marangoni convection in porous layers under oblique magnetic fields, highlighting the sensitivity of convection to external field orientation. Complementary studies on ferro convection in porous domains [4,6] have further underscored the interplay between magnetization, anisotropy, and permeability in controlling flow regimes.

Recent advancements have extended these classical and porous-medium models to nanofluids and hybrid nanofluid systems. Ahmed and Raizah [7] examined natural convection in variable-porosity media with nanofluid suspensions, while Kumar et al. [5] numerically investigated Marangoni-driven hybrid nanofluid flows over permeable stretching surfaces, revealing enhanced heat transfer and tuneable flow responses. Likewise, Shivakumara et al. [6] explored Brinkman–Bénard–Marangoni convection in magnetized ferrofluids, bridging the gap between microstructural physics and macroscopic transport. At a more fundamental level, analytical approaches have also established theoretical limits on heat transfer in high-Prandtl number regimes [8], reinforcing the mathematical underpinnings of Marangoni convection models.

Despite these advances, a unified understanding of coupled fluid–porous systems under Marangoni convection remains incomplete, particularly in configurations where layer thickness, permeability, couple-stress effects, and internal heating interact in nontrivial ways. Addressing these gaps is essential for optimizing thermal management, coating processes, and space-based fluid systems where buoyancy forces are suppressed. Motivated by these challenges, the present study develops analytical solutions for velocity and Marangoni convection in a fluid–porous layer system, systematically classifying the roles of enhancement, dampening, and weak parameters. By directly linking velocity distributions with surface-tension-driven convection behaviour, this work provides new insights into the stability and efficiency of coupled transport processes.

2. Mathematical Formulation

The physical configuration consists of a horizontal anisotropic porous layer of thickness d_m Underlying a fluid layer of thickness d with no lateral boundaries as shown in Fig.1. The lower boundary of anisotropic porous layer is taken to be rigid, while the upper free boundary of the fluid layer at which the surface tension acts is assumed to be non-deformable since for most liquid the capillary number is assumed to be very small, commonly ranging from $10^{-6} to 10^{-2}$. The surface tension σ is assumed to vary linearly with temperature in the form

$$\sigma = \sigma_0 - \sigma_T (T - T_0) \tag{1}$$

Where σ_0 is the unperturbed value and $-\sigma_T$ is the rate of change of surface tension with temperature .The temperature of the lower and upper boundaries is taken to be uniform and equal to T_l and T_u with $T_u < T_l$ .The Cartesian coordinates (x, y, z)is chosen such that the origin is at the interface between the fluid layer and the of anisotropic porous layer and the z-axis is vertically upward.

Governing Equation:

Fluid Layer:

$$\nabla \cdot V = 0 \tag{2}$$

$$\rho_0 \left[\frac{\partial \vec{V}}{\partial t} + \left(\vec{V} \cdot \nabla\right)\vec{V} \right] = -\nabla p + \mu \nabla^2 \vec{V} - \eta \nabla^4 \vec{V}) \tag{3}$$

$$\frac{\partial T}{\partial t}+\left(\vec{V}\cdot\nabla\right)T=\kappa\nabla^2T+q_f \tag{4}$$

Porous Layer:

$$\nabla_m\cdot V_m=0 \tag{5}$$

$$\frac{\rho_0}{\phi}\frac{\partial V_m}{\partial t}=-\nabla_m p_m-\mu K^{-1}.V_m \tag{6}$$

$$A\frac{\partial T_m}{\partial t}+\left(V_m\cdot\nabla_m\right)T_m=\nabla_m\cdot\left(\kappa_m\cdot\nabla_m T_m\right)+q_m \tag{7}$$

Here $\vec{V}$ is the velocity vector, p is the pressure, T is the temperature, and q_f is the heat source in the fluid layer, while V_m , p_m , T_m ,and q_m are corresponding quantities in the Porous Layer. κ is the thermal diffusivity , μ is the fluid viscosity, ϕ is the porosity of porous medium, A is the ratio of heat capacities, ρ_0 is the fluid density, K is the permeability tensor and κ_m is the thermal diffusivity tensor. The basic steady state is assumed to be quiescent and temperature distributions are found to be

$$T_b(z)=T_0-\left[\left(\frac{T_0-T_u}{d}\right)-\frac{q_f d}{2\kappa}\right]z+\frac{q_f}{2\kappa}z^2 \qquad 0\le z\le d$$

$$T_{mb}(z_m)=T_0-\left[\left(\frac{T_l-T_0}{d_m}\right)-\frac{q_m d_m}{2\kappa_{mv}}\right]z_m+\frac{q_m}{2\kappa_{mv}}z_m^{\,2} \qquad -d_m\le z_m\le 0 \tag{9}$$

$$\vec{V}=\vec{V}^{'}\ ,\ T=T_b(z)+T^{'},\ \ p=p_b(z)+p^{'} \tag{10}$$

$$\vec{V}_m=\vec{V}_m^{\,1},\quad T_m=T_{mb}(z)+T^{'}{}_m\ .\ p_m=p_{mb}(z)+p_m^{'} \tag{11}$$

Where the primed quantities are the perturbation assumed to be small. The Eqs. (10) and (11) are substituted in Eqs. (2)- (7) and linearized in the usual manner. T be pressure term is eliminated from Eqs. (3) and (6) by taking curl twice on these two equations and only the vertical component is retained. The variables are then non dimensionalized using $d,\frac{d^2}{\kappa},\frac{\kappa}{d}$ and T_o-T_u as the units of length, time, velocity, and temperature in the fluid layer and

$d_m, \frac{d_m}{\kappa_{mv}}^2, \frac{\kappa_{mv}}{d_m}$ and $T_l - T_o$ as the units of length, time, velocity, and temperature in the porous layer. The non-dimensional disturbance equations are given by

$$\left[\frac{\alpha^2}{\mathrm{Pr}}\frac{\partial}{\partial t} - \alpha^2\nabla^2 + \nabla^4\right]\nabla^2 w = 0 \tag{12}$$

$$\left[\frac{\partial}{\partial t} - \nabla^2\right]T = w\left[\left[1 - Ns_f(1-2z)\right]\right] \tag{13}$$

$$\left[\frac{Da}{\mathrm{Pr}_m}\frac{\partial}{\partial t} + \xi\nabla^2{}_{mh} + \frac{\partial^2}{\partial z^2{}_m}\right]w_m = 0 \tag{14}$$

$$\left[A\frac{\partial}{\partial t} - \eta\nabla^2{}_{mh} - \frac{\partial^2}{\partial z^2{}_m}\right]T_m = -w_m\left[1 + Ns_m(1+2z)\right] \tag{15}$$

Where $Da = \frac{K_v}{d^2{}_m}$ is the Darcy number, $Ns_f = \frac{q_f d^2}{2\kappa_v(T_0 - T_u)}$ & $Ns_m = \frac{q_m d_m{}^2}{2\kappa_{mv}(T_l - T_0)}$ are the dimensionless heat source strength in the fluid and porous layers respectively

$\mathrm{Pr} = \frac{\nu}{\kappa}$ is the Prandtl number, $\mathrm{Pr}_m = \frac{\nu\phi}{\kappa_{mv}}$ is the porous medium the Prandtl number

$\xi = \frac{K_h}{K_v}$ is the mechanical anisotropy parameter and $\eta = \frac{\kappa_{mh}}{\kappa_{mv}}$ is the thermal anisotropy parameter

K_h , K_v is the permeability in horizontal direction and vertical direction respectively,

κ_{mh}, κ_{mv} is the thermal diffusivity in horizontal direction and vertical direction respectively of porous medium.

The boundary conditions are:

$$w = \frac{\partial T}{\partial z} = 0 \; at \quad z = 1 \tag{16}$$

$$\frac{\partial^2 w}{\partial z^2} = M\nabla_h^2 T \; at \quad z = 1 \tag{17}$$

$$w_m = \frac{\partial T_m}{\partial z_m} = 0 \; at \quad z_m = -1 \tag{18}$$

Where, $M = \frac{\sigma_T(T_0 - T_u)d}{\mu\kappa}$ is the Marangoni number

At the interface (i.e., z=0) the normal component of velocity, temperature. Heat flux and normal stress are continuous. Since there is no viscous stress term in the Darcy equation, continuity of shear stress across the interface cannot be used. Instead, using slip condition proposed by Beavers and Joseph [1967]. Accordingly, the following condition at the interface is used.

$$w = \frac{\zeta}{\varepsilon_T} w_m \tag{19}$$

$$T = \frac{\varepsilon_T}{\zeta} T_m \tag{20}$$

$$\frac{\partial T}{\partial Z} = \frac{\partial T_m}{\partial Z_m} \tag{21}$$

$$\left[3\nabla_h^{\,2} + \frac{\partial^2}{\partial z^2}\right]\frac{\partial w}{\partial z} = -\frac{\zeta^4}{\varepsilon_T Da\xi}\frac{\partial w_m}{\partial z_m} \tag{22}$$

$$\frac{\partial^2 w}{\partial z^2} = \frac{\beta\zeta}{\sqrt{Da\xi}}\frac{\partial w}{\partial z} - \frac{\beta\zeta^3}{\varepsilon_T\sqrt{Da\xi}}\frac{\partial w_m}{\partial z_m} \tag{23}$$

where $\varepsilon_T = \frac{\kappa}{\kappa_{mv}}$ is the ratio of thermal diffusivities β is the slip parameter and

$\nabla_h^{\,2} = \frac{\partial^2}{\partial x^2} + \frac{\partial^2}{\partial y^2}$ is the horizontal Laplacian operator.

$$(w, T) = [W(z), \Theta(z)]\exp[i(lx + my)] \tag{24}$$

$$(w_m, T_m) = [W_m(z), \Theta_m(z)]\exp\left[i\left(\tilde{l}x + \tilde{m}y\right)\right] \tag{25}$$

$$\left(D^2 - a^2\right)^2\left(D^2 - b^2\right)W = 0 \tag{26}$$

$$\left(D^2 - a^2\right)\Theta = -W\left[1 - Ns_f(1 - 2z)\right] \tag{27}$$

$$\left(D_m^2 - \xi a_m^2\right)W_m = 0 \tag{28}$$

$$\left(D_m^2 - \eta a_m^2\right)\Theta = -W_m\left[1 + Ns_m(1 + 2z)\right] \tag{29}$$

Where D and D_m are differentiation with respect to z and z_m respectively, $a = \sqrt{l^2 + m^2}$ and $a_m = \sqrt{\tilde{l}^2 + \tilde{m}^2}$ are correspondingly overall horizontal wave number in the fluid and porous layers and $\frac{a}{d} = \frac{a_m}{d_m}$ as the wave numbers must be same in the fluid and porous layers.

Hence $\zeta = \frac{a}{a_m}$

The twelve boundary conditions become

$$W = \left(D^2 - a^2\right) W = D\Theta = 0 \qquad \text{at z = 1} \tag{30}$$

$$D^2 W + Ma^2 \Theta = 0 \tag{31}$$

Those at the interface (z=0) are:

Method of solution: Exact solution

Solving equation (26) and (27), we get the general solution in the form

$$W = \left(A_1 + A_2 z\right)\cosh az + \left(B_1 + B_2 z\right)\sinh az + A_3 \cosh bz + B_3 \sinh bz \tag{32}$$

$$W_m = A_{m1} \cosh\left(\sqrt{\xi} a_m z_m\right) + A_{m2} \sinh\left(\sqrt{\xi} a_m z_m\right) \tag{33}$$

$$\Theta = C_1 \cosh az + C_2 \sinh az - \left(1 - Ns_f\right)\left[\begin{array}{l} A_1 \frac{z}{2a}\cosh az + A_2\left(\frac{z^2}{4a} - \frac{z}{4a^2}\right)\cosh az + B_1 \frac{z}{2a}\sinh az + \\ B_2\left(\frac{z^2}{4a} - \frac{z}{4a^2}\right)\sinh az + A_3 \frac{1}{b^2 - a^2}\cosh bz + B_3 \frac{1}{b^2 - a^2}\sinh bz \end{array}\right]$$

$$+2\left[\begin{array}{l} A_1\left(\frac{z^2}{4a} - \frac{z}{4a^2}\right)\cosh az + A_2\left(\frac{z^3}{6a} - \frac{z^2}{4a^2} + \frac{z}{4a^3}\right)\cosh az + B_1\left(\frac{z^2}{4a} - \frac{z}{4a^2}\right)\sinh az \\ + B_2\left(\frac{z^3}{6a} - \frac{z^2}{4a^2} + \frac{z}{4a^3}\right)\sinh az + A_3\left(\frac{z^2}{b^2 - a^2} - \frac{2b}{\left(b^2 - a^2\right)^2}\right)\cosh bz + B_3\left(\frac{z^2}{b^2 - a^2} - \frac{2b}{\left(b^2 - a^2\right)^2}\right)\sinh bz \end{array}\right] \tag{34}$$

Where $A_1 - A_3$, $B_1 - B_3$, $A_{m1} and\ A_{m2}$ are constants determined using the boundary conditions to obtain W and W_m

$$W = A_2[R \cosh az + z \cosh az + G \sinh az + Ez \sinh az + \lambda \cosh bz + Q \sinh bz] \tag{35}$$

$$W_m = A_2\left[N \cosh\left(\sqrt{\xi} a_m z_m\right) + N \sinh\left(\sqrt{\xi} a_m z_m\right) \coth\left(\sqrt{\xi} a_m\right)\right] \tag{36}$$

Using the coupled boundary condition (31), an expression for Marangoni number is finally obtained in the form

$$M = \frac{-1}{a^2}\left[\frac{\cosh a\left(a^2R + a^2 + 2aE\right) + \sinh a\left[2a + Ga^2 + a^2E\right] + \cosh b\left[b^2\lambda\right] + \sinh\left[b^2Q\right]}{K_{71}\cosh a + K_{72}\sinh a + K_{73}\cosh b + K_{74}\sinh b}\right] \quad (37)$$

Where

$$\Delta_1 = \frac{\zeta}{\xi_T}$$

$$K = \frac{-\zeta^4}{Da\,\xi_T\,\xi}$$

$$K_1 = \frac{\beta\zeta}{\sqrt{Da\,\xi}}$$

$$K_2 = \frac{-\beta\zeta^3}{\sqrt{Da\,\xi}\,\xi_T}$$

$$K_{11} = K\sqrt{\xi}\,a_m$$

$$K_{12} = K_{11}\coth\sqrt{\xi}\,a_m$$

$$K_{21} = K_2\sqrt{\xi}\,a_m$$

$$K_{22} = K_{21}\coth\sqrt{\xi}\,a_m$$

$$L_2 = K_{11}\sinh\sqrt{\xi}\,a_m + K_{12}\cosh\sqrt{\xi}\,a_m$$

$$L_3 = K_{21}\sinh\sqrt{\xi}\,a_m + K_{22}\cosh\sqrt{\xi}\,a_m$$

$$E_1 = \left[-\left(1 - NS_f\right)\left(\frac{1}{2a}\right) + \left(\frac{1}{2a} - \frac{1}{2a^2}\right)\right]$$

$$E_2 = \left[-\left(1 - NS_f\right)\left(\frac{1}{4a} - \frac{1}{4a^2}\right) + \left(\frac{1}{3a} - \frac{1}{2a^2} + \frac{1}{2a^3}\right)\right]$$

$$E_3 = \left[-\left(1 - NS_f\right)\left(\frac{1}{b^2 - a^2}\right) + \left(\frac{2}{b^2 - a^2} - \frac{4b}{\left(b^2 - a^2\right)^2}\right)\right],$$

$$K_{71} = H + RE_1 + E_2,$$

$$K_{72} = F + GE_1, \quad K_{73} = \lambda E_3, \quad K_{74} = Q\,E_3$$

$$b^2 = \alpha^2 + a^2$$

Figures

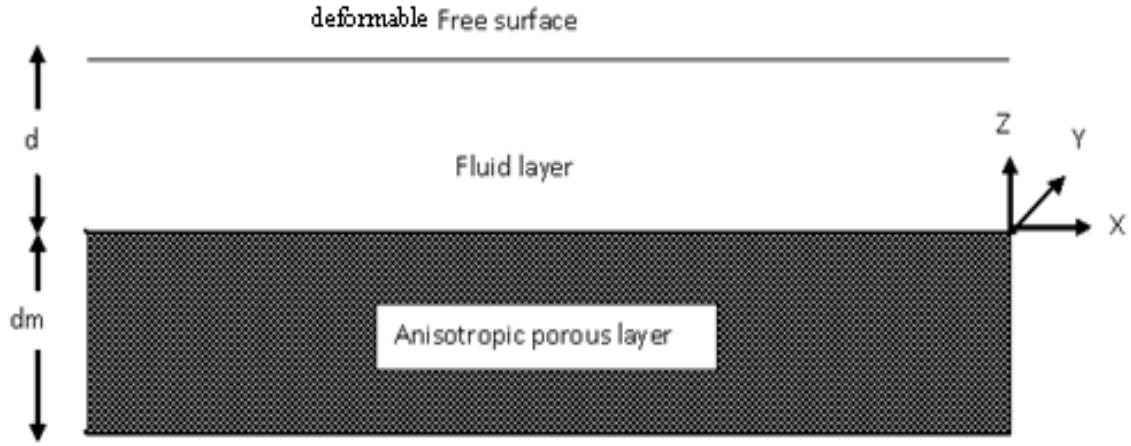

Figure 1: Physical configuration of the problem

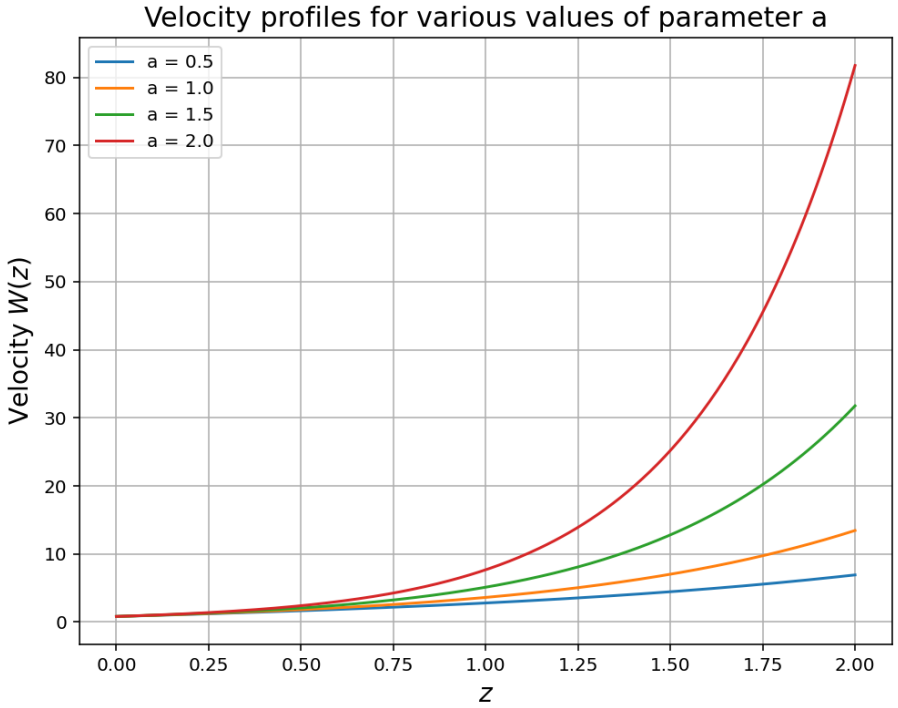

Figure 2: Velocity profiles for varying values of "a"

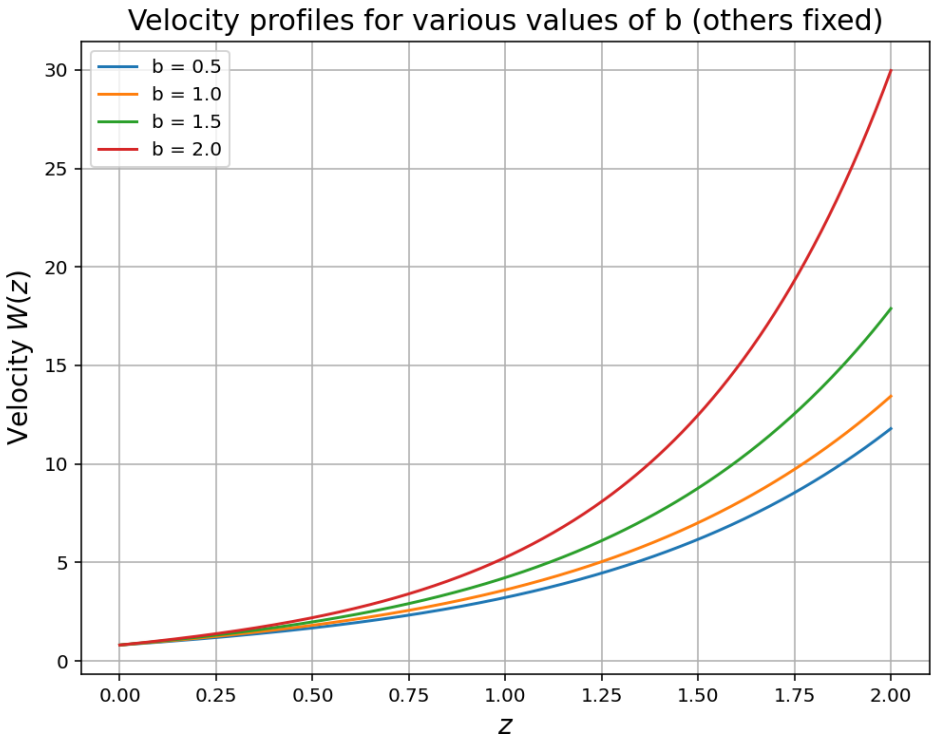

Figure 3: Velocity profiles for varying values of "b"

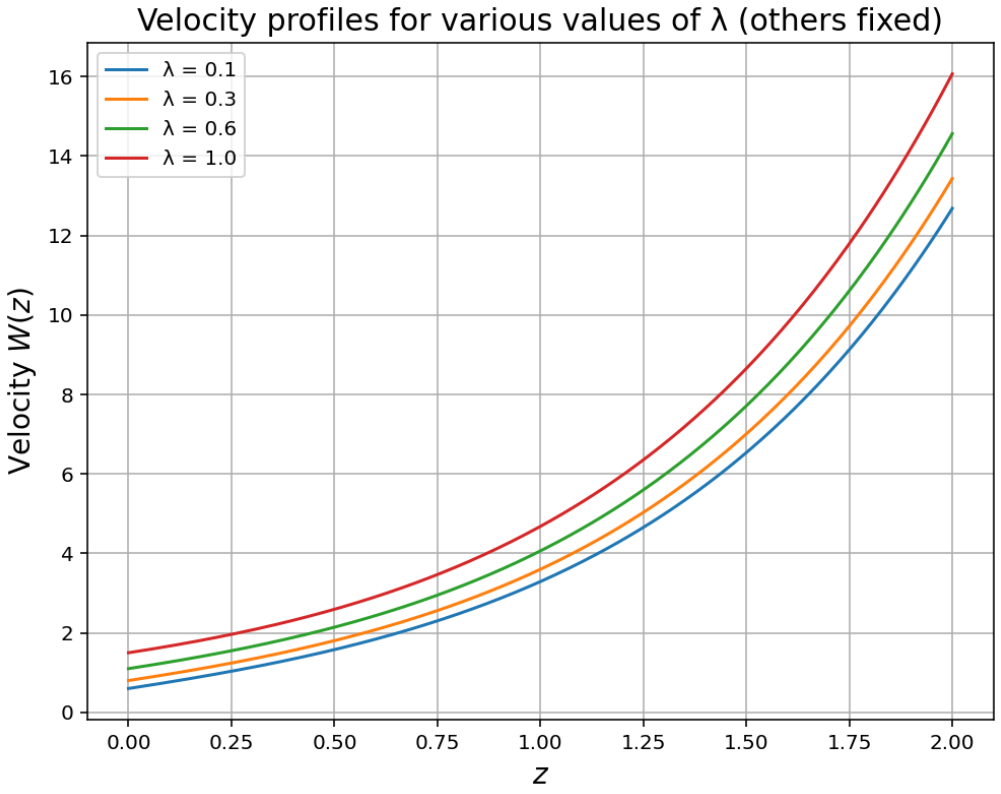

Figure 4: Velocity profiles for varying values of " λ "

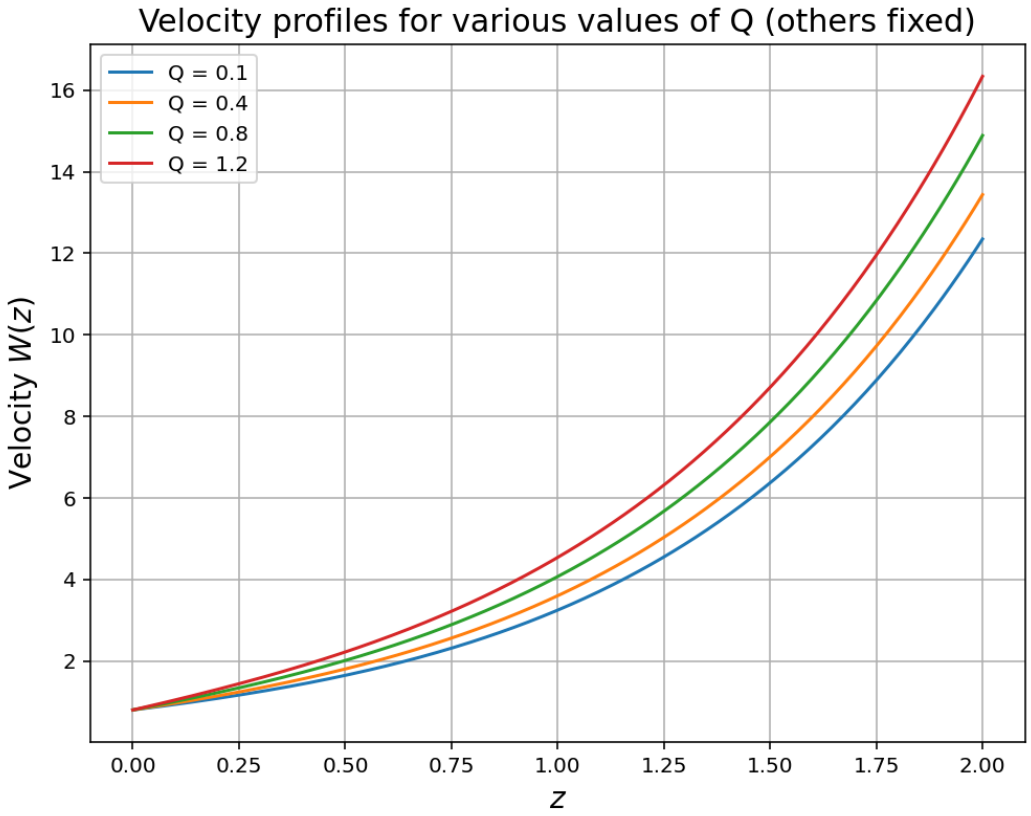

Figure 5: Velocity profiles for varying values of " Q "

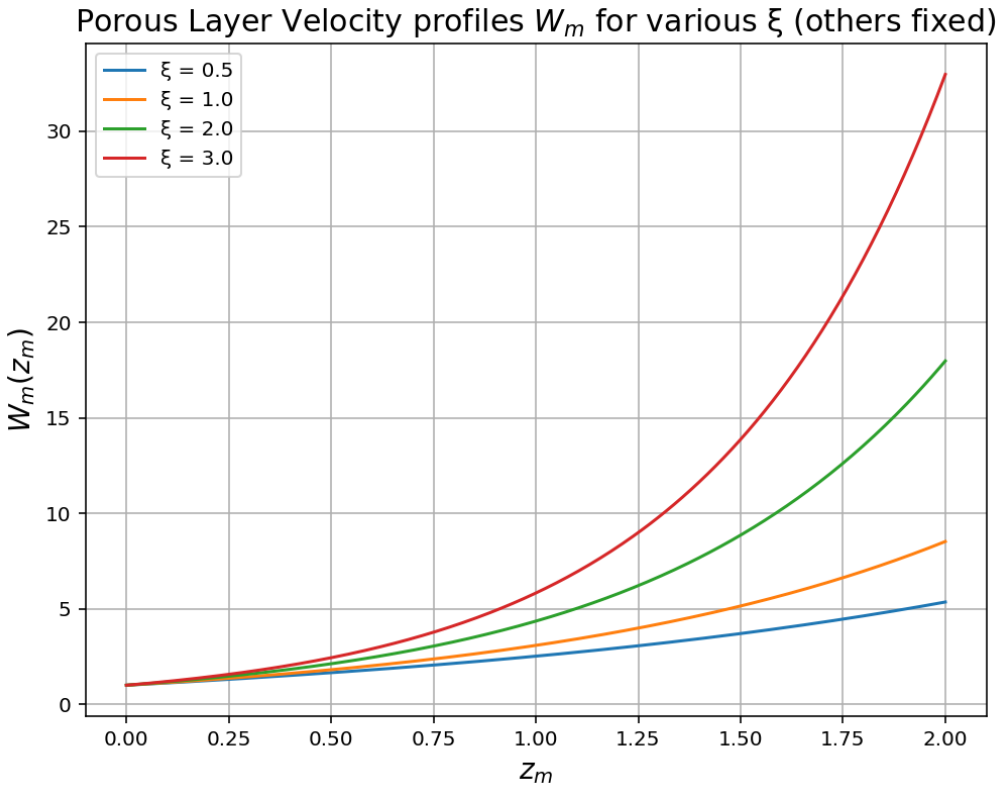

Figure 6: Porous layer velocity profiles for varying values o " ξ "

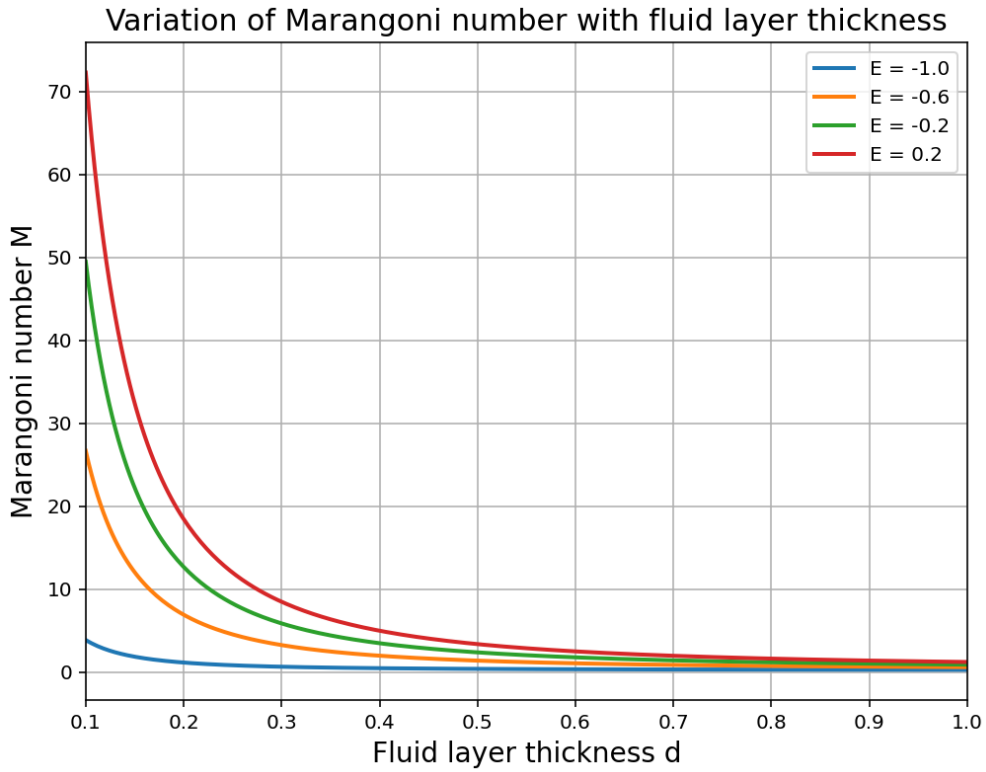

Figure 7: Variation of Marangoni number for varying values of " E"

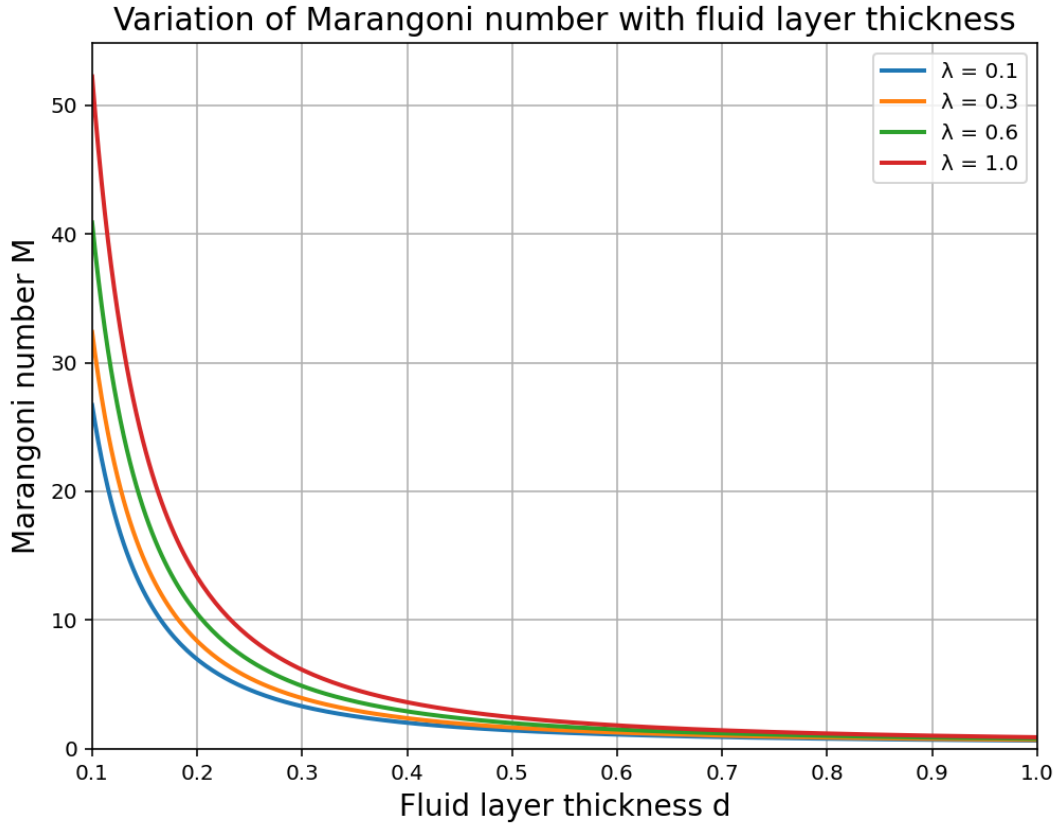

Figure 8: Variation of Marangoni number for varying values of "λ"

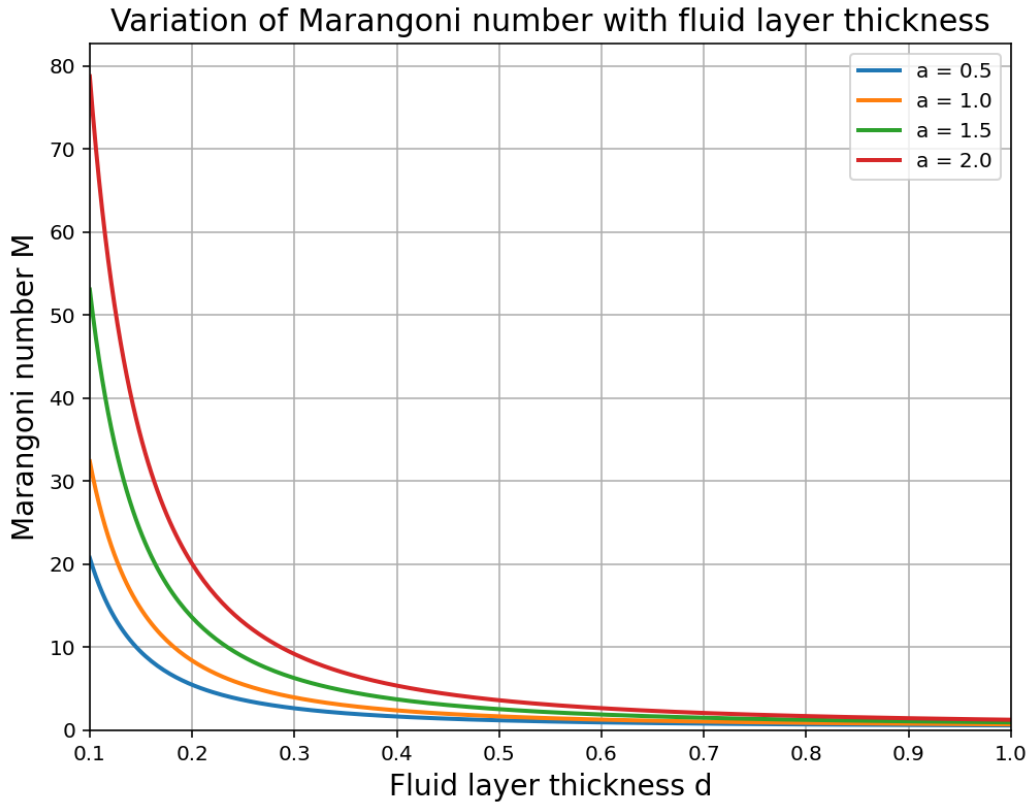

Figure 9: Variation of Marangoni number for varying values of "a"

3. Results and Discussion

The analytical solutions obtained provide valuable insights into velocity distributions in both the fluid and porous layers, as well as the variations of the Marangoni number under different parametric conditions. The results are presented in Figures 2–9.

3.1 Velocity Profiles

Figure 2 illustrates the influence of parameter a on velocity $W(Z)$ in the fluid layer. Velocity increases significantly with higher a, reaching nearly fourfold enhancement compared to the baseline case. This nonlinear growth suggests that a functions as a strong driving parameter, likely associated with couple-stress effects, where a reduction in couple-stress resistance enhances fluid acceleration due to increased particle spin.

Figure 3 demonstrates the effect of parameter b. Although it also enhances velocity, its contribution is more moderate, with peak velocities roughly one-third of those observed for parameter a. The closer spacing of velocity curves indicates that a acts as a secondary scaling factor, possibly of geometric origin.

Figure 4 presents the variation of velocity with parameter λ. Unlike a and b, increasing λ consistently suppresses velocity profiles, with reductions nearly by half between the smallest

and largest tested values. This confirms that λ represents a resistance parameter, linked to viscous drag or permeability opposition, which stabilizes the flow.

Figure 5 depicts the influence of Q, showing only marginal changes in velocity. The velocity curves remain closely clustered across the entire range, indicating that Q plays a weak role, possibly related to boundary heating conditions or secondary forcing.

Figure 6 shows the porous layer velocity $W_m(Z_m)$ as a function of ξ. Here, velocity grows strongly with increasing ξ, from around 8 units at $\xi = 0.5$ to nearly 30 units at $\xi = 3.0$. This behaviour confirms that ξ governs permeability effects, promoting stronger transport in the porous medium and acting analogously to the enhancing role of parameters a and b in the fluid layer.

3.2 Marangoni Number Variations

Figure 7 presents the dependence of Marangoni number M on fluid layer thickness d for various E. All profiles show exponential decay, consistent with theoretical predictions that surface-tension-driven convection dominates thin layers but weakens rapidly as thickness increases. Less negative values of E sustain higher M, reaching nearly 70 when $d \leq 0.1$.

Figure 8 shows the influence of λ on the Marangoni number. Increasing λ suppresses M across all thicknesses, confirming its stabilizing effect. At small thicknesses, $M \approx 50$ for $\lambda = 0.1$, but drops significantly at higher λ, mirroring the dampening effect observed in velocity profiles.

Figure 9 highlights the effect of parameter a on Marangoni convection. Consistent with its role in enhancing velocity, larger a values yield markedly higher Marangoni numbers, particularly for thin layers where convection is strongest. Maximum M values approach 80 at $a = 2.0$, reinforcing the strong coupling between momentum enhancement and surface-tension effects.

3.3 Interpretation and Implications

Overall, the parameters can be classified into three categories: (i) enhancement factors (a, b, ξ) that increase both velocity and Marangoni number, (ii) a dampening factor (λ) that consistently suppresses flow and convection, and (iii) a weak factor (Q) with negligible influence. The exponential decay of Marangoni number with layer thickness reaffirms that thin fluid layers are most effective for sustaining thermocapillary convection.

These findings hold practical significance. Thin layers $(d < 0.3)$ ensure strong Marangoni effects, while parameters such as a and ξ may be tuned to enhance system performance. Conversely, λ must be carefully controlled to prevent excessive suppression of convective transport.

4. Conclusion

In this study, exact analytical solutions were obtained for the onset of Marangoni convection in a fluid layer overlying an anisotropic porous medium, subject to the combined influences of internal heat generation and couple stresses. The closed-form results enabled a systematic exploration of parameter effects on velocity distributions and the critical Marangoni number.

The analysis reveals that enhancement-related parameters (a,b, and ξ) increase both velocity and the Marangoni number, while the resistance parameter (λ) has a stabilizing influence by suppressing flow strength. The couple-stress parameter is shown to diminish velocity, indicating that weaker couple stresses promote stronger thermocapillary motion. Internal heat generation consistently amplifies convection in the fluid layer, though its effect within the porous medium depends sensitively on the relative thickness of the layers. Furthermore, the Marangoni number decreases almost exponentially with increasing fluid-layer thickness, underscoring the role of geometry in modulating surface-tension-driven instabilities.

Overall, the derived exact solutions provide valuable benchmarks for studying thermocapillary transport in fluid–porous systems. The findings offer physical insight into the interplay between heat generation, couple stresses, and anisotropic porous structures, with potential relevance to thermal management technologies, microgravity fluid mechanics, and advanced coating processes.

References

1. R Kozak, M.Z Saghir, A Viviani, *Marangoni convection in a liquid layer overlying a porous layer with evaporation at the free surface*, Acta Astronautica, Volume 55, Issues 3–9, 2004, Pages 189-197, https://doi.org/10.1016/j.actaastro.2004.05.017
2. Saghir, M., Islam, M., and Legros, J., *Transient Convection Flow in Super-Imposed Fluid and Porous Layers*, SAE Technical Paper 2000-01-2322, 2000, https://doi.org/10.4271/2000-01-2322.
3. Abdullah, A.A., Rashed, Z.Z. *Instability of the Benard–Marangoni Convection in a Porous Layer Affected by a Non-Vertical Magnetic Field*. *J Appl Mech Tech Phy* **59**, 903–911 (2018). https://doi.org/10.1134/S0021894418050188
4. Nor Halawati Senin, Nor Fadzillah Mohd Mokhtar, and Mohamad Hasan Abdul Sathar. 2024. *Ferroconvection in an Anisotropic Porous Medium With Variable Gravity*. *Journal of Advanced Research in Fluid Mechanics and Thermal Sciences* 71 (2):56-68. https://semarakilmu.com.my/journals/index.php/fluid_mechanics_thermal_sciences/article/view/6283.
5. Deepak Kumar, Priyanka Agrawal, Praveen Kumar Dadheech, Qasem Al-Mdallal, *Numerical study of Marangoni convective hybrid-nanofluids flow over a permeable stretching surface*, International Journal of Thermofluids, Volume 23, 2024, 100750, ISSN 2666-2027, https://doi.org/10.1016/j.ijft.2024.100750.
6. I.S. Shivakumara, Jinho Lee, C.E. Nanjundappa, M. Ravisha, *Brinkman–Benard–Marangoni convection in a magnetized ferrofluid saturated porous layer*, International Journal of Heat and Mass Transfer, Volume 53, Issues 25–26, 2010, Pages 5835-5846, ISSN 0017-9310, https://doi.org/10.1016/j.ijheatmasstransfer.2010.07.064.
7. S E Ahmed, Z A S Raizah. *Natural Convection Flow of Nanofluids in a Composite System with Variable-Porosity Media. Journal of Thermophysics and Heat Transfer, 2018, 32(2), 495-502. https://doi.org/10.2514/1.T5311*.

8. Fantuzzi G, Pershin A, Wynn A. Bounds on heat transfer for Bénard–Marangoni convection at infinite Prandtl number. *Journal of Fluid Mechanics*. 2018;837:562-596. doi:10.1017/jfm.2017.858
9. Scriven LE, Sternling CV. *On cellular convection driven by surface-tension gradients: effects of mean surface tension and surface viscosity*. *Journal of Fluid Mechanics*. 1964;19(3):321-340. doi:10.1017/S0022112064000751
10. Koschmieder EL, Biggerstaff MI. *Onset of surface-tension-driven Bénard convection*. *Journal of Fluid Mechanics*. 1986;167:49-64. doi:10.1017/S0022112086002720.